JOURNAL OF PETROLOGY | VOLUME 47 | NUMBER 11 | PAGES 2105–2122 | 2006 | doi:10.1093/petrology/egl038

Extreme U–Th Disequilibrium in Rift-Related Basalts, Rhyolites and Granophyric Granite and the Timescale of Rhyolite Generation, Intrusion and Crystallization at Alid Volcanic Center, Eritrea

J. B. LOWENSTERN[1]*, B. L. A. CHARLIER[2], M. A. CLYNNE[1] AND J. L. WOODEN[3]

[1]VOLCANO HAZARDS TEAM, MAIL STOP 910, US GEOLOGICAL SURVEY, 345 MIDDLEFIELD ROAD, MENLO PARK, CA 94025, USA

[2]DEPARTMENT OF EARTH SCIENCES, THE OPEN UNIVERSITY, WALTON HALL, MILTON KEYNES MK7 6AA, UK

[3]EARTH SURFACE PROCESSES TEAM, MAIL STOP 937, US GEOLOGICAL SURVEY, 345 MIDDLEFIELD ROAD, MENLO PARK, CA 94025, USA

RECEIVED SEPTEMBER 20, 2005; ACCEPTED JUNE 14, 2006; ADVANCE ACCESS PUBLICATION JULY 14, 2006

Rhyolite pumices and co-erupted granophyric (granite) xenoliths yield evidence for rapid magma generation and crystallization prior to their eruption at 15·2 ± 2·9 ka at the Alid volcanic center in the Danikil Depression, Eritrea. Whole-rock U and Th isotopic analyses show ^{230}Th excesses up to 50% in basalts <10 000 years old from the surrounding Oss lava fields. The 15 ka rhyolites also have 30–40% ^{230}Th excesses. Similarity in U–Th disequilibrium, and in Sr, Nd, and Pb isotopic values, implies that the rhyolites are mostly differentiated from the local basaltic magma. Given the ($^{230}Th/^{232}Th$) ratio of the young basalts, and presumably the underlying mantle, the ($^{230}Th/^{232}Th$) ratio of the rhyolites upon eruption could be generated by in situ decay in about 50 000 years. Limited (~5%) assimilation of old crust would hasten the lowering of ($^{230}Th/^{232}Th$) and allow the process to take place in as little as 30 000 years. Final crystallization of the Alid granophyre occurred rapidly and at shallow depths at ~20–25 ka, as confirmed by analyses of mineral separates and ion microprobe data on individual zircons. Evidently, 30 000–50 000 years were required for extraction of basalt from its mantle source region, subsequent crystallization and melt extraction to form silicic magmas, and final crystallization of the shallow intrusion. The granophyre was then ejected during eruption of the comagmatic rhyolites.

KEY WORDS: *U-series; zircon; ion microprobe; volcano; geochronology*

INTRODUCTION

Although volcanic eruptions can be fleeting events, characterized by explosive or effusive activity lasting only hours or days at a time, the time necessary to create the erupted magma is far longer. Although basaltic magmas may migrate from their mantle origins to the surface quickly, typically within hundreds or thousands of years (Condomines *et al.*, 1988; McKenzie, 2000), silicic magmas generally have more protracted lifespans (Reid, 2003). Some researchers contend that the crystallization and assimilation processes necessary to create voluminous silicic magmas may take hundreds of thousands of years (Reagan *et al.*, 2003). Others infer more rapid creation and migration of silicic melts (Harris *et al.*, 2000; Petford *et al.*, 2000). In general, small-volume, shallow silicic bodies might be expected to crystallize more rapidly than larger, deeper ones because of rapid heat loss and consequent crystallization. Until now, only a few studies have assessed the duration of magma genesis for small-volume silicic melts, usually constraining the timing of fractionation

*Corresponding author. Telephone: 1-650-329-5238. Fax: 1-650-329-5203. E-mail: jlwnstrn@usgs.gov

from intermediate to silicic magmas and without final solidification (e.g. Black *et al.*, 1997; Heumann & Davies, 2002).

The U-decay series has proven to be a sensitive indicator of the timescale for magma genesis (Allègre, 1968; Gill *et al.*, 1992; Hawkesworth *et al.*, 2001; Reid, 2003). The timing of magma extraction and differentiation is often constrained with decay series sensitive for timescales of $\leq \sim$7500 years for ^{226}Ra to $\leq$350 000 years for ^{230}Th. Most such studies focus on identifying time-correlative trends in the whole-rock isotopic compositions of consanguineous lavas (e.g. Cooper *et al.*, 2001; Reagan *et al.*, 2003; Rogers *et al.*, 2004). Other studies identify age populations of crystals to infer magma residence times within the crust (Reid *et al.*, 1997; Vazquez & Reid, 2002) or the ages of crystal populations inherited from remelted intrusions (Bindeman *et al.*, 2001; Schmitt *et al.*, 2003; Miller & Wooden, 2004; Charlier *et al.*, 2005). Combining such techniques, one might be able to determine the timing of both melt generation and crystallization. The timing of intrusion and solidification can be studied directly when volcanic systems erupt comagmatic granitoid blocks that represent key time controls on magma genesis (Bacon *et al.*, 2000; Lowenstern *et al.*, 2000; Charlier *et al.*, 2003; Bacon & Lowenstern, 2005).

Lowenstern *et al.* (1997) described such xenoliths of granophyric composition (granite) that were the quenched intrusive equivalents of co-erupted tephras, vented at ~20 ka at the Alid volcanic center, Eritrea. Initial intrusion of the granitic magma caused inflation of the Alid volcanic center (a structural dome) around 35 000 years ago. The excellent constraints on the timing of shallow intrusion, crystallization and eruption make this system ideal for a geochronological study of the time necessary for magma generation and crystallization prior to eruption as xenoliths. In this paper we use secondary ion mass spectrometry (SIMS) studies of crystals, as well as isotopic studies of phenocryst separates and whole-rocks, to deduce the history of the rhyolites and shallow granophyre and related young basalts. We find that the silicic magma probably was generated by fractional crystallization of basaltic magma, and that the entire time for basalt extraction from the mantle, intrusion into the upper crust, differentiation to rhyolite and final solidification was less than ~50 000 years. Crystallization of the granophyre itself appears to have taken less than 20 000 years.

BACKGROUND GEOLOGY

Alid volcanic center and the Danakil Depression

The Alid volcanic center, Eritrea (Marini, 1938; Duffield *et al.*, 1997; Lowenstern *et al.*, 1999) is located along the axis of the Danakil Depression, the graben trace of a crustal spreading center that radiates NNW from a plate-tectonic triple junction within a complexly rifted and faulted basaltic lowland called the Afar Triangle (Fig. 1). The Danakil Depression is a subaerial segment of the spreading system that is opening to form the Red Sea. It lies near or below sea level for much of its extent and is surrounded by the Danakil Alps to the east and the Eritrean plateau to the west, which rises to elevations up to ~2600 m above sea level. Both of these bordering regions are underlain primarily by Pan-African basement composed of Precambrian gneisses, granites and schists, and are typically covered by mid-Tertiary basalts and rhyolites. Much of the Afar lowland is covered with Pliocene and Quaternary lavas (CNR–CNRS, 1973). Erta Ale, one of the most active volcanoes in the world, lies about 100 km SE of Alid.

The Alid volcanic center is an elliptical structural dome formed during uplift caused by shallow intrusion of rhyolitic magma, some of which was erupted as pumice (Duffield *et al.*, 1997). The major axis of Alid is 7 km long, elongated ENE–WSW, perpendicular to the trend of the (Danakil) graben (Fig. 1). The minor axis is about 5 km long, parallel to the graben. Alid rises ~700 m above a field of Late Pleistocene and Holocene basaltic lavas, the Oss basalts [*yb* in Table 1 and Duffield *et al.* (1997)], which lap unconformably against the north and south flanks of the Alid dome. The youngest of these lavas have much less vegetation than on neighboring Alid and have undergone negligible (if any) geomorphological change since eruption. Marini (1938) reported seeing gaseous emissions from a cinder cone in the southern Oss field during an expedition in 1902.

The oldest rocks that crop out on Alid are basement Precambrian quartz–mica and kyanite schists exposed within a deep canyon, Sillaló, that drains the east side of the mountain (Fig. 2). Overlying this basement rock is the 'sedimentary sequence' (*ss*), consisting of shallow-water marine siltstone and sandstone, pillow basalt, subaerial basalt, anhydrite beds and fossiliferous limestone, all interpreted to be of Pleistocene age (Duffield *et al.*, 1997). The 'sedimentary sequence' is found on all parts of the structural dome, and dips radially away from its geographic center. Stratigraphically above the 'sedimentary sequence' is the 'lava shell' (*ls*), which consists of basalt (*sb*) and basaltic andesite lava flows, pyroclastic deposits, amphibole-bearing rhyolite domes, and intercalated aeolian sands. One amphibole-bearing rhyolite was dated by Duffield *et al.* (1997) at 212 ± 19 ka. The shell rocks form most of the slopes of the mountain, with dips locally as steep as 65°. Such steep dip slopes must have formed subsequent to emplacement of these fluid lava flows, as they are far too steep to be original (Duffield *et al.*, 1997).

Table 1: *Major element, trace element and isotopic composition of whole-rocks from the Alid volcanic center and surrounding Oss basalts*

Sample no.:	C7	D11	D1	S9	C42	C15	D3	C21	C25
Map unit:	*yb*	*yb*	*sb*	*yb*	*frhy1*	*pf/pxrhy*	*frhy3*	*pf*	*pf-inc*
SiO_2	49·80	50·80	51·10	54·73	72·50	73·20	73·31	73·50	73·63
Al_2O_3	16·10	15·09	16·39	14·73	13·56	13·45	13·17	13·12	13·20
FeO*	10·99	10·79	9·45	11·30	2·94	2·53	2·79	2·52	2·42
MgO	5·89	6·88	6·67	3·23	0·13	0·23	0·02	0·18	0·16
CaO	11·11	10·05	10·58	6·83	1·17	0·85	0·77	0·97	0·98
Na_2O	2·69	2·82	2·90	3·97	4·67	4·64	4·94	4·20	4·54
K_2O	0·86	1·04	0·97	2·00	4·55	4·69	4·58	5·11	4·69
TiO_2	1·77	1·71	1·26	2·20	0·26	0·23	0·20	0·23	0·23
P_2O_5	0·34	0·37	0·29	0·55	0·04	0·05	0·03	0·04	0·04
MnO	0·19	0·19	0·18	0·21	0·12	0·06	0·11	0·07	0·06
LOI	−0·23	−0·14	−0·24	0·09	3·58	0·72	0·71	2·47	0·60
Mg-no.	54·4	58·7	61·1	38·9	8·7	17·2	1·6	13·5	13·0
U (ppm)	0·655	0·735	0·599	1·428	3·728	3·425	3·995	3·688	2·478
±2σ	0·002	0·002	0·002	0·005	0·009	0·012	0·010	0·020	0·003
Th (ppm)	2·375	2·712	2·295	4·894	13·650	14·102	14·547	14·208	12·495
±2σ	0·022	0·024	0·020	0·078	0·091	0·103	0·072	0·102	0·100
$(^{234}U/^{238}U)_{act}$	1·002	1·010	1·012	1·005	1·006	1·002	1·000	1·000	1·007
±2σ	0·005	0·006	0·006	0·008	0·005	0·007	0·004	0·008	0·004
$(^{238}U/^{232}Th)_{act}$	0·836	0·822	0·792	0·886	0·829	0·737	0·833	0·788	0·602
±2σ	0·008	0·008	0·007	0·015	0·006	0·006	0·005	0·007	0·005
$(^{230}Th/^{232}Th)_{act}$	1·305	1·251	1·124	1·220	1·008	1·076	0·994	1·073	1·064
±2σ	0·010	0·013	0·009	0·009	0·010	0·008	0·010	0·009	0·008
$(^{230}Th/^{238}U)_{act}$	1·560	1·522	1·420	1·378	1·216	1·460	1·192	1·363	1·768
±2σ	0·013	0·016	0·012	0·012	0·013	0·012	0·013	0·014	0·014
$^{87}Sr/^{86}Sr$	0·70333	0·70332	0·70323	0·70338	0·70440	0·70388	0·70382	0·70441	0·70468
$^{143}Nd/^{144}Nd$			0·512817	0·512801				0·512820	
$^{206}Pb/^{204}Pb$			19·608	19·409	19·256			19·214	19·213
$^{207}Pb/^{204}Pb$			15·659	15·621	15·609			15·618	15·616
$^{208}Pb/^{204}Pb$			39·412	39·086	38·880			38·879	38·871
Li	4·44	5·39	5		11·34	15·15	22·21	14	21
P	1245	1431			106	108	43		
Sc	29	27	35		4	6	6	5	6
V	352	333	349		2	6	1	47	52
Cr	93·9	222·2			2·31	2·26	2·01		
Co	37·5	38·1	44		0·37	1·07	0·10	1	1
Ni	50·5	86·5	50		0·51	1·30	0·33	0	1
Rb	15	17	20		99	102	106	118	112
Sr	357	317	455		75	46	29	47	42
Y	18	23	19		53	51	62	58	55
Zr	75	94	82		380	*413*	454	*408*	*413*
Nb	31	34	31		113	112	131	118	122
Cs	0·154	0·170	0·175		1·247	0·958	1·294	1·218	0·238
Ba	273	317	356		860	563	903	476	494
La	21·4	23·9	20·6		73·7	96·2	85·8	74·4	71·6
Ce	42·9	48·1	40·8		141·4	226·3	170·0	137·8	134·7
Pr	4·9	5·6			15·3	19·5	17·9		

Table 1: continued

Sample no.:	C7	D11	D1	S9	C42	C15	D3	C21	C25
Map unit:	*yb*	*yb*	*sb*	*yb*	*frhy1*	*pf/pxrhy*	*frhy3*	*pf*	*pf-inc*
Nd	19·4	21·9	18·3		53·9	65·1	63·2	55·6	54·2
Sm	3·76	4·31	3·64		9·61	10·80	11·34	9·99	9·91
Eu	1·25	1·37	1·21		1·59	1·24	1·64	1·15	1·13
Tb	0·55	0·65			1·41	1·46	1·67		
Gd	3·58	4·24	3·54		8·64	9·03	10·29	9·48	9·54
Dy	3·20	3·93	3·23		8·60	8·51	10·20	9·33	9·05
Ho	0·64	0·79			1·79	1·70	2·13		
Er	1·8	2·3	1·9		5·5	5·1	6·4	8·8	5·2
Tm	0·28	0·35			0·88	0·81	1·03		
Yb	1·71	2·11	1·85		5·63	5·06	6·52	6·01	4·70
Lu	0·27	0·33	0·31		0·89	0·78	1·03	0·89	0·64
Hf	1·87	2·35	1·95		9·33	9·73	10·72	9·63	9·32
Ta	2·03	2·20	1·96		7·00	7·32	8·17	8·23	8·25
Pb	1·70	1·99	2·00		9·18	8·26	10·15	9·26	5·30

Major element analysis at USGS, Denver (analyst D. Siems). Data normalized to 100% anhydrous, including FeO and Fe_2O_3 as calculated by Duffield *et al.* (1997). Mg-number = 100 × Mg/(Mg + Fe) as reported by Duffield *et al.* (1997). Map units defined in text and by Duffield *et al.* (1997). U and Th analyses by isotope dilution, U–Th activity ratios by TIMS: both at Open University by B. L. A. Charlier. U–Th activity ratios calculated with decay constants listed by Charlier *et al.* (2003). Pb isotopic analyses reprinted from Duffield *et al.* (1997). Sr and Nd analyses from this study and Duffield *et al.* (1997). Trace element analysis at USGS, Menlo Park by inductively coupled plasma-mass spectrometry (ICP-MS; analyst J. Fitzpatrick) except where shown in italics (XRF at Washington State University). LOI, loss on ignition.

Structural doming and magma intrusion

Structural doming caused considerable distension of the shell and sedimentary units and effected landsliding and collapse of the central region of the mountain, resulting in a basin-like depression at the summit. The onset of structural doming at Alid postdates about 36 ka, the age of a basalt flow stratigraphically high within the sequence of uplifted rocks (Duffield *et al.*, 1997). Clinopyroxene-bearing rhyolite lavas (some with minor fayalite) erupted subsequent to the initiation of structural doming [*frhy3* of Duffield *et al.* (1997)], and one of these lavas is dated at 33·5 ± 4·6 ka. Other similar fayalite-bearing lavas erupted during the structural doming (groups *frhy1* and *2*); the relative timing of the three groups of rhyolitic lavas (*frhy1*, *2* and *3*) is uncertain, and they may have been contemporaneous. Ultimately, fayalite-absent (but still clinopyroxene-bearing) pyroclastic flows (*pf*) vented from the summit region and today form blankets of tephra up to 15 m thick in the summit basin and on the west flank of Alid. The final phase of this climactic eruption (sample C15), a vent-clogging lava flow, was dated by Duffield *et al.*, (1997) at 23·5 ± 1·9 ka based on Ar–Ar geochronology on feldspar separates. The sample was separated out as unit *pxrhy* by Duffield *et al.* (1997), but is shown in Fig. 2 as part of the *pf* unit. Later in this paper, we reinterpret the geochronological data as indicating a slightly younger eruption age of 15·2 ± 2·9 ka for the climactic eruption (*pf*) and its immediately post-eruptive lava flow.

Duffield *et al.* (1997) concluded that a body of granitic magma intruded to a shallow level, caused structural doming, and erupted as lava flows and pyroclastic deposits. Lowenstern *et al.* (1997) described granophyric xenoliths within the climactic pyroclastic flow deposits (*pf*). The xenoliths (*pf-inc*) and host tephras had nearly identical petrographic, chemical and isotopic characteristics, causing Lowenstern *et al.* to conclude that the xenoliths were the solidified intrusive equivalents of the tephra. The granophyre contains predominant phenocrysts of feldspar, ranging from Na-sanidine to anorthoclase, quartz, ferroaugite, minor biotite, titanomagnetite, and the accessory phases zircon, chevkinite, apatite, sulfide, and fluorite [see Lowenstern *et al.* (1997) for more detailed petrographic information and mineral analyses]. The host pumice deposits contain an identical mineralogy except for the biotite, zircon, chevkinite and fluorite, which are interpreted to be near-solidus reaction products within the granophyre (phenocryst grain mounts from the pumice were searched exhaustively for zircon using the backscatter detector on an electron microscope). Both rocks contain about 40% phenocrysts relative to 60% groundmass (either glassy or

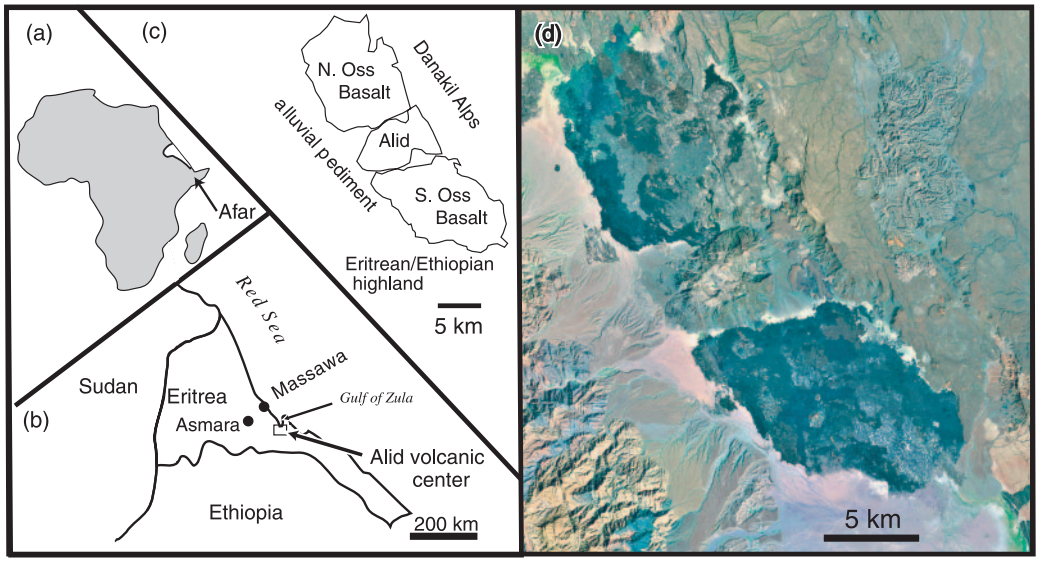

Fig. 1. Location maps of the Alid volcanic center. North is toward the top of the page in all maps. (a) Eritrea (white area) is outlined in NE Africa. Arrow points to general location of the Afar lowland. (b) Alid volcanic center is located about 20 km south of the Gulf of Zula and 90 km SE of the port city of Massawa, Eritrea. (c) Sketch map outlining geological units shown in (d). (d) A Thematic Mapper satellite image of the field area within the Danakil Depression.

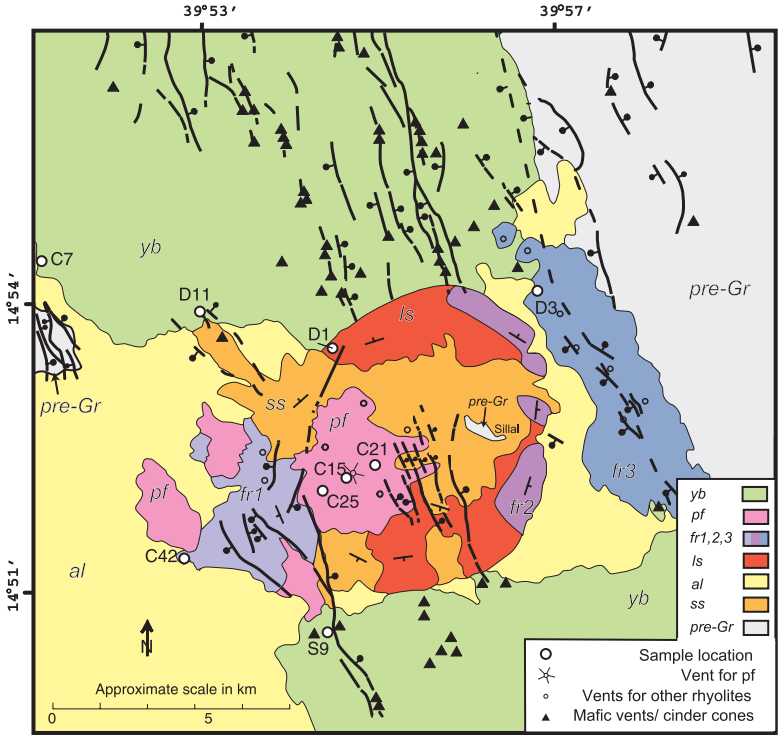

Fig. 2. Simplified geological map of the Alid volcanic center, modified from Duffield *et al.* (1997). Unit names as in text; *frhy* units are abbreviated to *fr*. Pre-graben rocks are denoted as pre-Gr and consist of Precambrian and Tertiary rocks plus Pleistocene lavas erupted prior to spreading in this part of the Danakil Depression. Pleistocene rocks on Alid include *ss*, containing marine sediments and intercalated basalts, and *ls* (the lava shell), with young basaltic lavas (*sb* in Table 1) and other pre-Alid, subaerial volcanic rocks. Faults are continuous lines (dashed where inferred) with balls on the downthrown side.

granophyric). About 85% of the crystals in both rocks are feldspar; quartz, pyroxene and titano-magnetite make up the remainder of the phenocryst population. Phenocrysts in the pumice are remarkably euhedral, although evidence for some early (and overgrown) resorption can be seen by careful petrographic analysis (e.g. Lowenstern *et al.*, 1997, fig. 4). Other rhyolite groups [*frhy1*, *frhy2*, *frhy3* of Duffield *et al.* (1997, figs 2 and 4)] have slightly different mineralogy in that they contain fayalite and are sparsely phyric (<10–15% crystals).

To reiterate, Lowenstern *et al.* (1997) concluded that the granophyric xenoliths represent crystallized equivalents of rhyolitic magmas erupted at the Alid volcanic center, and are most closely related to the fayalite-absent *pf* unit in which they are found.

Geochemistry and petrology

Rock chemistry and textures of the surrounding Oss basalt fields were described by Duffield *et al.* (1997). These flat-lying lavas of the rift floor contain a variety of textures, ranging from sparsely phyric to porphyritic. The latter contain phenocrysts of olivine alone, olivine plus plagioclase, or olivine plus plagioclase plus clinopyroxene. In some units, plagioclase phenocrysts >1 cm long are present. Groundmasses are typically very fresh with textures that range from glassy to aphanitic and rarely holocrystalline. The rocks are subalkalic to alkalic basalts and basaltic andesites with hypersthene-normative compositions that define a tholeiitic differentiation trend; incompatible trace element concentrations are relatively high compared with mid-ocean ridge basalt (MORB) (Fig. 3, Table 1). There are no systematic chemical differences between the Oss basalts and the young basalts (*sb*) found on the Alid structural dome.

The Oss–Alid volcanism is essentially bimodal, as rock types intermediate between rhyolite and basalt are rare and, where present, show signs of magma mixing (Duffield *et al.*, 1997). Most such mixed samples were found as inclusions within lava flows and pumice deposits, not as independently erupted units. Pumice and quenched inclusions ranging from 54·8 to 64·5 wt % SiO_2 are minor components of the climactic *pf* deposits, which are otherwise dominated by rhyolite pumice and ash with 73 wt % SiO_2.

Isotopic analyses of Sr, Pb, and Nd (Table 1, and Duffield *et al.*, 1997) show some variation within the range of erupted basalts, but far less than is evident in the regional range of values, strongly implying that incorporation of Precambrian crust was very limited, even in the rhyolites which have relatively similar isotopic compositions to the basalts [see Duffield *et al.* (1997) and see Discussion below].

ANALYTICAL METHODS

Zircons were separated and prepared as discussed by Lowenstern *et al.* (2000) and analyzed in both March and October 2001, on the SIMS (SHRIMP-RG) at Stanford University. Using a 30 nA $^{16}O^-$ or $^{16}O_2^-$ primary ion beam, a 50 μm × 40 μm rectangular region was rastered for 2 min to remove the Au coat and surface contamination. A flat-floored elliptical pit (40 μm × 25 μm × 2 μm) was excavated into the zircon. Data were collected for $^{90}Zr_2^{16}O$, ^{232}Th, ^{238}U, $^{230}Th^{16}O$, background ($^{230}Th^{16}O$ + 0·05 a.m.u.), $^{232}Th^{16}O$, and $^{238}U^{16}O$. Scan times ranged from 2 to 15 s for each peak. Counts were added together without curve-fitting or any other statistical technique and errors were propagated by standard techniques assuming that the counting error for each peak was equal to the square root of the number of counts.

A U–Th fractionation factor (f) for each analytical session was empirically determined through repeated analysis of AS57, a 1·1 Ga zircon sample from the Duluth Complex, Minnesota (Paces & Miller, 1993). ^{238}U and ^{230}Th activities for such old zircons should be at secular equilibrium. By constraining them onto the equiline, f can be derived and then applied to the younger zircons. We determined f values of 1·077 (March 2001) and 0·995 (October 2001) and used them to calculate ($^{238}U/^{232}Th$) of young zircons of unknown age (Charlier *et al.*, 2003). Our estimated 1σ uncertainty for f is 3%, which is greater than the analytical error by counting statistics alone and contributes to a relatively conservative estimate of the $^{238}U/^{232}Th$ of the samples (Bacon & Lowenstern, 2005; Charlier *et al.*, 2005). U concentrations were estimated by comparison of $^{238}U/Zr_2O$ for the sample relative to a zircon standard of known U concentration [SL13 (238 ppm) or CZ3 (550 ppm)]. Th concentrations were calculated by multiplying the U concentration of the sample by the product of f and the analyzed $^{232}Th^{16}O^+/^{238}U^{16}O^+$ concentration ratio. Standards were measured every fourth or fifth analysis. Zircon ^{238}U–^{230}Th model ages were calculated as two-point isochrons between the zircon analysis and the whole-rock (Reid *et al.*, 1997). Decay constants were those used by Charlier *et al.* (2003).

Thermal ionization mass spectrometry (TIMS) analyses were performed on whole-rocks and mineral separates at the Open University, UK, on a Finnegan MAT 262 mass spectrometer using an RPQ-II energy filter. The ($^{230}Th/^{232}Th$) external reproducibility was monitored by repeat analyses of an in-house standard, Th'U'std (van Calsteren & Schweiters, 1995), which gave $^{230}Th/^{232}Th = 6{\cdot}14 \pm 0{\cdot}12 \times 10^{-6}$ (1·92% 2 SD; $n = 74$) during the course of this study. The in-house uranium standard (U456) gave $^{234}U/^{236}U = 0{\cdot}09752 \pm 0{\cdot}5$ 2σ%

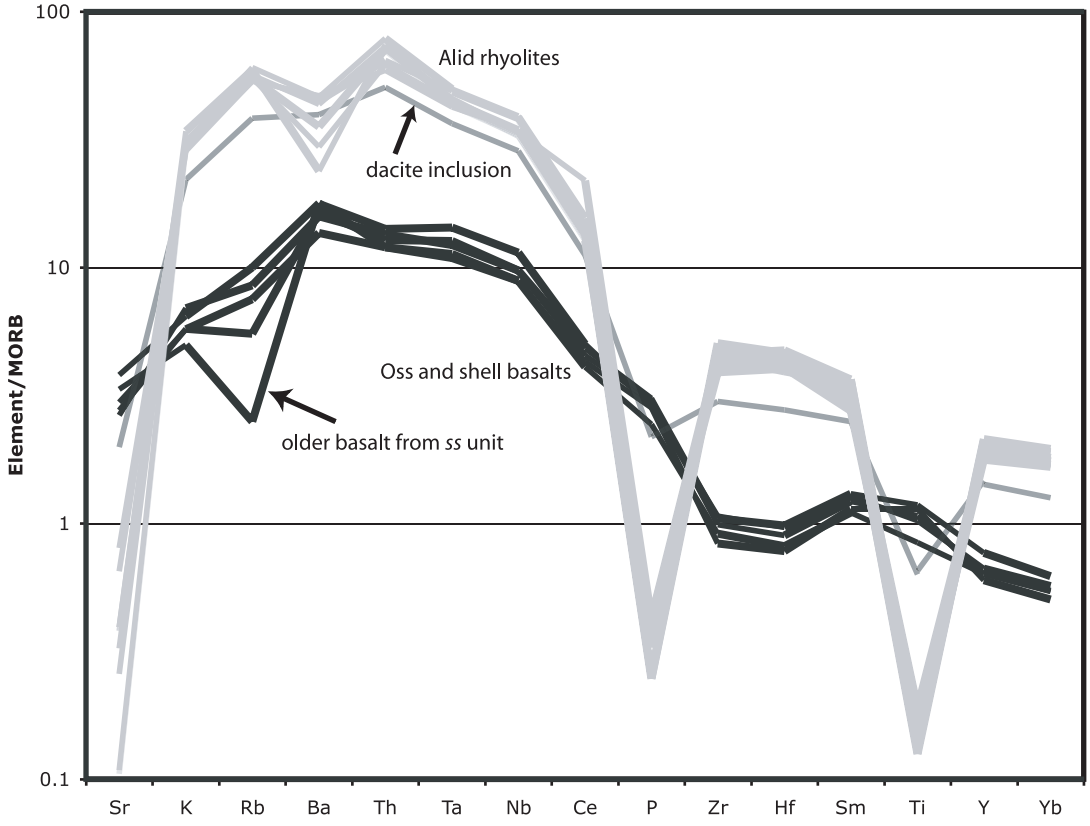

Fig. 3. MORB-normalized trace element diagrams (Pearce, 1983) for representative young basalts and rhyolites from the Alid volcanic center and vicinity. The dacite inclusion is from the *pf* unit.

and $^{235}U/^{236}U = 13{\cdot}26466 \pm 0{\cdot}36$ 2σ% ($n = 93$). Six repeat determinations of the AThO standard gave ($^{230}Th/^{232}Th$) = 1·0260 ± 1·33 2σ% and ($^{238}U/^{232}Th$) = 0·9465 ± 1·84 2σ%. Procedural blanks were <100 pg for both U and Th, and are considered negligible compared with the >100 ng of sample generally loaded. Further information has been given by Charlier *et al.* (2005) and references therein.

Sr, Nd, and Pb isotopic analyses were performed in Menlo Park, CA (USA) according to techniques described by Bullen & Clynne (1990). Most of the Sr and all the Pb analyses in Table 1 were originally published by Duffield *et al.* (1997).

RE-EVALUATING THE AGE OF THE *pf* ERUPTION

Duffield *et al.* (1997) estimated an age of 23·5 ± 1·9 ka for the most recent pyroclastic eruption of the Alid volcanic center (*pf*), which brought the granophyric xenoliths (*pf-inc*) to the surface. That $^{40}Ar/^{39}Ar$ age was based on pooling the results of analyses (total fusion by laser) of four feldspar separates from the vent-clogging rhyolitic flow (sample C15) extruded at the end of the eruption. Two separates consisted of feldspar with density <2·59 g/cm^3. These samples yielded disparate ages at 1σ of 23·9 ± 3·8 and 33·5 ± 3·2 ka. Two other separates with density >2·59 g/cm^3 provided ages of 16·2 ± 4·6 and 14·5 ± 3·7 ka. Besides the older apparent ages, the lower-density sample had higher K/Ca consistent with feldspar rims and granophyric groundmass. We suspect that the older ages reflect the presence of excess Ar, resulting in spurious and inconsistent data, whereas the two young ages are in good agreement. The anorthoclase-rich fraction (denser) more reliably reflects the age of the eruption than the Na-sanidine overgrowths that apparently grew in a shallow gas-rich environment (Layer & Gardner, 2001) atop the magma chamber at Alid (Lowenstern *et al.*, 1997). We consider the weighted mean of the two denser feldspar fractions to yield the best estimate of the eruption age of the *pf* eruption, 15·2 ± 2·9 ka.

SIZE OF THE SHALLOW MAGMA CHAMBER

Given the areal extent of the structural dome at the Alid volcanic center, we can estimate the volume of the probably now-crystallized intrusion remaining below. The 5 km × 7 km structure is certainly underlain by a

shallow (<2–3 km depth) intrusion and would thus have a diameter of between 3 and 5 km (Lowenstern *et al.*, 1997). A minimum estimate for the size of the intrusion would follow from a 3 km diameter and a laccolithic geometry, giving a total volume of about 7 km^3. A maximum estimate assumes a spherical intrusion with a 5 km diameter, giving a volume of 65 km^3. Even the smaller volume is much greater than the total amount of silicic magma so far erupted at Alid, which is ~1 km^3. As such, the amount of felsic magma intruded and erupted at Alid over the past 35 000 years is probably 10–50 km^3, and the intrusive/extrusive ratio is in the range 10–50. Given the areal extent of the Oss basalts and their estimated thickness (50 m), probably no more than 10 km^3 of basalt erupted around the periphery of Alid during the same time period.

CRYSTALLIZATION AGES WITHIN THE ALID GRANOPHYRE

Zircon ages by SIMS

We analyzed 36 spots within 31 different zircon crystals from a single hand-sample over two separate sessions (Table 2). Uranium concentrations ranged from ~300 to >8000 ppm, with some zircons showing considerable zoning (Fig. 4). Spots lower in U tended to have slightly older apparent ages, though their analytical error was also greater (Fig. 5). A simple best-fit isochron through the zircon data yielded an age of 26 500 ± 5300 years (2σ) with an MSWD of 1·7 and a probability of 0·009 (calculated with Isoplot 3.0; Ludwig, 2003*a*). The low probability implies that some zircons crystallized outside of this 10 000 year window (Ludwig, 2003*b*), or that there are unidentified sources of analytical error. Several zircons cross to the left of the equiline, implying that the melt phase was Th enriched. Indeed, TIMS analysis of the whole-rock sample of the granophyre (C25 in Table 1, WR in Table 3) indicates a 77% Th excess [($^{230}Th/^{238}U$) = 1·77].

Using the whole-rock value together with individual zircon analyses allows calculation of two-point isochrons or model ages for each zircon spot. The inset in Fig. 5 shows a histogram of the slopes of these isochrons. About two-thirds of the analyzed spots have slopes to the whole-rock composition between 0·15 and 0·25, corresponding to ages of ~17·7 to 31·3 ka. The oldest zircon spot is 65·6 ka (+15·7, – 13·7, 1σ) with the exception of a single grain with a ^{238}U–^{206}Pb age of 760 Ma, which is certainly derived from the Pan-African basement.

TIMS ages of zircons and other phenocryst phases

U–Th isotopic analyses of mineral separates (feldspar, pyroxene, magnetite, apatite and zircon) and whole-rock powder from the Alid granophyre form an isochron of 21·5 ka ± 2·4 ka (2σ error, with MSWD of 1·8 and probability of 0·09) that lies astride the zircon data (Fig. 6). An isochron through the major phenocryst phases alone, not including zircons, gives a value of 17·0 ± 6·0 ka (2σ, with MSWD of 0·78 and probability of 0·50). The isotopic composition of the phenocrysts and whole-rock powder reveals that the entire rock is out of equilibrium in the U–Th system. The whole-rock powder has a 77% ^{230}Th excess. Three zircon separates, analyzed by TIMS, had ($^{238}U/^{232}Th$) between 1·8 and 2·2, with similar U concentrations around 1100 ppm (Table 3). They plot very close to the isochrons formed by the SIMS zircon analyses and represent a homogeneous population of zircons without a significant range of ages (see Charlier & Zellmer, 2000).

U-SERIES WHOLE-ROCK RESULTS FOR NEARBY RHYOLITES AND BASALTS

Nine other young volcanic rocks from the Alid volcanic center and the surrounding Oss basalts were analyzed for their U-series systematics; all displayed significant disequilibrium (Table 1). In the basalts, the Th excess reaches a maximum of 56%, slightly greater than that seen in basalts from the Asal rift, which erupted in 1978 (Vigier *et al.*, 1999). Disequilibrium is prevalent as well in the rhyolites. As shown in Fig. 7, two rhyolitic samples, inflated pumice (*pf*, sample C21) and the vent-clogging flow from the 15·2 ka pyroclastic eruption (*pf*, sample C15) plot close to the isochron for the granophyre. These two young rhyolites have 36 and 46% excess ^{230}Th, respectively. Two older rhyolitic samples, an aphyric pumice (C42 from *frhy1*) and a lava dome [sample D3 from *frhy3* of Duffield *et al.* (1997)], both estimated to have erupted at 30–36 ka, plot at lower ($^{230}Th/^{232}Th$), closer to the equiline, but still with 19 and 21% excess ^{230}Th and at similar U/Th to the other rhyolitic rocks from Alid.

The very young basaltic rocks from the Oss field and Alid volcanic center have U/Th similar to the rhyolites so that all analyzed rocks form a linear vertical trend in Fig. 7. The oldest dated basalt, D1 (*sb*, shown within *ls* in Fig. 2), is estimated to have erupted immediately prior to doming (~36 ka) and plots close to the best-fit line for the granophyre mineral separates. At the time of eruption, it would have had ($^{230}Th/^{232}Th$) of ~1·25, slightly less than the youngest Oss basalts analyzed. The sample highest in ($^{230}Th/^{232}Th$) is a porphyritic plagioclase basalt with ($^{230}Th/^{232}Th$) of 1·305.

Table 2: *SIMS analyses of zircons from Alid granite (*pf-inc, *C25)*

Spot no.	Run no.	U (ppm)	Th (ppm)	(238/232)	±1σ	(230/232)	±1σ	Slope	±1σ	Tm (ka)	σ+ (ka)	σ– (ka)
1.1	1	2200	3600	1·90	0·06	1·32	0·06	0·196	0·047	23·8	6·6	6·2
2.1	1	2700	5100	1·66	0·05	1·31	0·05	0·236	0·047	29·3	6·9	6·5
3.1	1	300	300	3·18	0·10	1·70	0·24	0·245	0·095	30·6	14·6	12·9
4.1	1	800	1000	2·72	0·08	1·76	0·13	0·329	0·065	43·4	11·1	10·0
5.1	1	4800	6300	2·35	0·07	1·33	0·05	0·150	0·027	17·7	3·6	3·4
5.3	2	7300	9100	2·50	0·08	1·37	0·04	0·160	0·021	18·9	2·8	2·7
6.1	1	500	400	3·71	0·11	2·08	0·23	0·328	0·073	43·3	12·6	11·3
6.2	2	1100	900	3·50	0·11	1·46	0·18	0·136	0·064	15·9	8·3	7·7
7.1	1	2500	5700	1·39	0·04	1·26	0·05	0·247	0·064	30·9	9·6	8·8
7.2	2	400	1000	1·20	0·04	1·19	0·04	0·210	0·064	25·6	9·1	8·4
8.1	1	3400	5700	1·84	0·06	1·35	0·06	0·228	0·051	28·1	7·4	6·9
9.1	1	500	500	3·59	0·11	1·74	0·22	0·226	0·074	27·9	10·9	9·9
10.1	1	5300	9300	1·78	0·05	1·28	0·04	0·186	0·034	22·3	4·7	4·5
11.1	1	2800	4500	1·98	0·06	1·22	0·05	0·110	0·040	12·7	5·1	4·8
12.1	1	3400	4400	2·44	0·07	1·45	0·06	0·211	0·034	25·8	4·8	4·6
14.1	1	400	400	3·54	0·11	1·94	0·25	0·298	0·086	38·4	14·2	12·5
15.1	1	3700	6200	1·88	0·06	1·34	0·05	0·216	0·042	26·4	6·0	5·7
17.1	1	400	300	3·92	0·12	1·83	0·24	0·229	0·073	28·3	10·7	9·8
18.1	1	1400	2300	1·85	0·06	1·22	0·07	0·129	0·057	15·0	7·3	6·9
19.1	1	500	600	2·83	0·09	1·72	0·19	0·293	0·086	37·7	14·1	12·5
20.1	1	400	300	4·12	0·12	1·87	0·26	0·229	0·074	28·3	10·9	9·9
21.1	1	900	1100	2·45	0·07	1·90	0·13	0·453	0·073	65·7	15·7	13·7
22.1	1	800	800	3·05	0·09	1·47	0·15	0·165	0·060	19·6	8·1	7·5
23.1	1	600	1700	1·12	0·03	1·22	0·08	0·297	0·159	38·3	27·8	22·1
24.1	1	2200	2100	3·33	0·10	1·70	0·10	0·234	0·036	29·1	5·3	5·1
24.2	2	2900	2800	3·24	0·10	1·57	0·08	0·190	0·030	22·9	4·1	4·0
25.1	1	800	800	3·05	0·09	1·73	0·15	0·273	0·063	34·7	9·9	9·1
27.2	2	8200	11200	2·29	0·07	1·29	0·04	0·135	0·025	15·8	3·2	3·1
28.2	2	6500	9400	2·18	0·07	1·30	0·04	0·149	0·028	17·5	3·6	3·5
30.2	2	8100	10900	2·32	0·07	1·36	0·04	0·171	0·024	20·4	3·2	3·1
30.3	2	4100	4500	2·85	0·09	1·43	0·07	0·161	0·030	19·1	3·9	3·8
31.1	2	500	400	3·93	0·12	1·78	0·29	0·217	0·088	26·5	12·9	11·5
32.1	2	5600	17400	1·01	0·03	1·12	0·03	0·130	0·072	15·2	9·4	8·6
33.1	2	8200	26000	0·99	0·03	1·06	0·02	-0·008	0·064	-0·8	7·2	6·7
34.1	2	4100	7000	1·86	0·06	1·31	0·05	0·193	0·041	23·4	5·7	5·4
35.1	2	3600	4900	2·30	0·07	1·45	0·06	0·226	0·040	27·9	5·7	5·4

Spot number: value before period indicates crystal number; value after period indicates replicate analysis of that crystal. Run 1 was carried out in March 2001; Run 2 in October 2001. U and Th concentrations in ppm by weight. Error ±10%. (238/232): activity ratio of $^{238}U/^{232}Th$. Decay constants used to calculate values have been listed by Charlier *et al.* (2003). ±1σ: the one sigma uncertainty of the activity ratio or slope. Slope: slope of the line connecting the zircon analysis with the assumed melt value of (230/232) = 1·064, (238/232) = 0·602; used to calculate age. Tm: model age (in ka) calculated from the slope of a two-point isochron between the zircon analysis and assumed melt value listed above. σ+ (ka): the 1σ upper age uncertainty calculated with the age equation, propagating the error in the slope. σ– (ka): the 1σ lower age uncertainty calculated with the age equation, propagating the error in the slope.

DISCUSSION

Rapid crystallization of the granophyre

Virtually all the zircons within the granophyre crystallized within the same time period as doming and volcanism at the Alid volcanic center (36–15 ka). Notwithstanding the obvious zoning in some zircons from the Alid granophyre (Fig. 4), we find little evidence for a protracted crystallization history for any individual grains (e.g. Fig. 4f and grains 5,7, and 30) or the

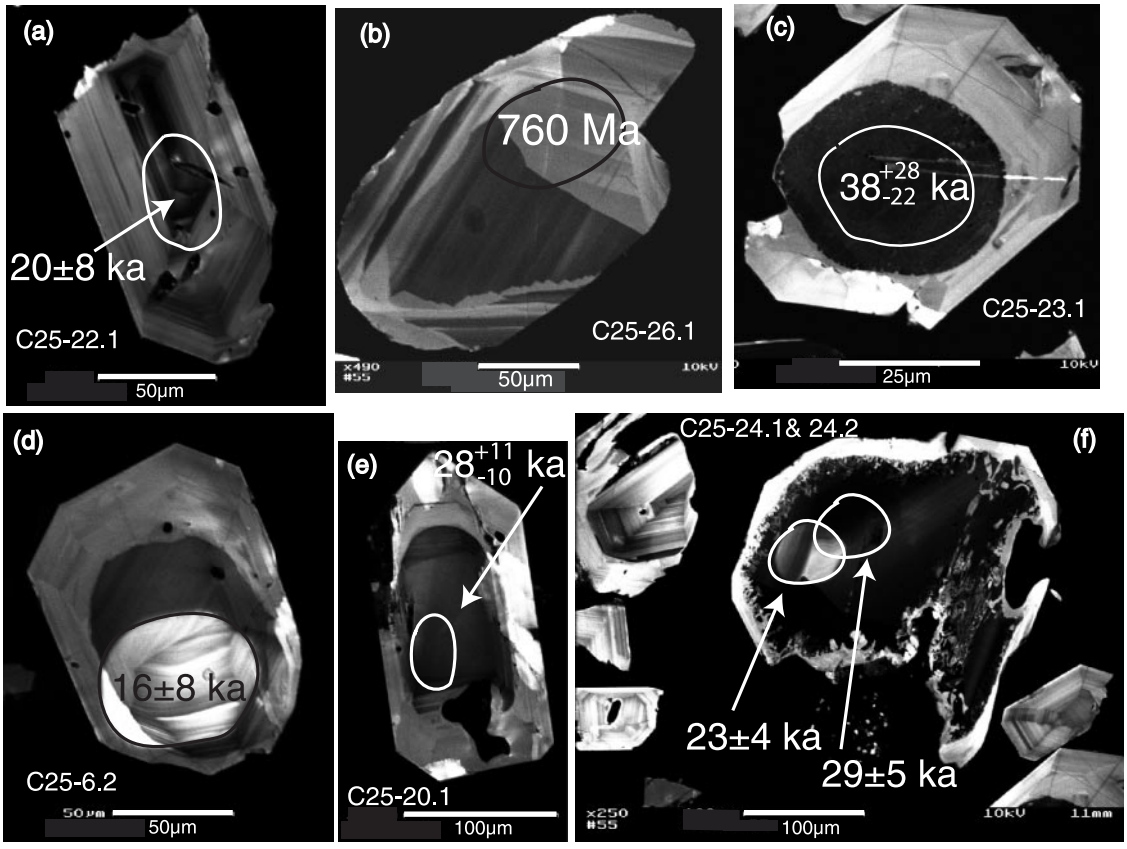

Fig. 4. Cathodoluminescence images of zircons separated from C25, a granitic xenolith from the 15·2 ka pyroxene rhyolite pumice deposit at Alid volcanic center. Variations in the color of the zircon crystals correlate with zonation in U concentration, where darker colors equate with high U. The approximate area of analysis is outlined with a white or black ellipse, and the determined age is indicated. In (d) and (f) the image was obtained after analysis but prior to re-coating with Au, causing the analyzed region to appear white. All other images were taken either prior to analysis or after repolishing and re-coating with Au.

population as a whole. The apparent absence of zircon in the host pumice deposits further implies that zircon grew rapidly late in the crystallization history of the granophyre as it solidified along the walls of the shallow magma chamber (Lowenstern *et al.*, 1997). Moreover, the other phenocryst phases plot on essentially the same isochron as the zircons. The similarity between the zircon data, the phenocryst data, and the known eruption age implies that essentially all crystallization of the granophyre occurred less than 20 000 years before its eruption as a xenolith in the pyroclastic flow. The slightly older apparent ages of the low-U zircons (Fig. 5) may signify that early formed zircons grew from less differentiated magma 10 000–15 000 years prior to final solidification. However, the larger errors associated with the low-U spots make such an assertion difficult to confirm. The lower U/Th of the granophyre relative to the rhyolite probably reflects zircon (and apatite) fractionation along the walls of the magma chamber, creating locally Th-enriched melts such as the granophyre. The presence of small (late-formed) chevkinite inclusions within or attached to larger phenocrysts may be responsible for the slightly lower U/Th of the feldspar, pyroxene and magnetite separates compared with the whole-rock. Overall, the data are consistent with the major phenocrysts growing in a shallow intrusion after initial formation of the structural dome. As concluded by Lowenstern *et al.* (1997) crystallization of the granophyric groundmass, including some of the zircon growth, probably occurred by quenching as a result of degassing during pre-*pf* volcanic eruptions at Alid (e.g. *frhy1*, *2*, and *3*).

Generating extreme disequilibrium in the Alid–Oss magmas

All analyzed volcanic rocks, both rhyolites and basalts, display considerable U/Th disequilibrium and ^{230}Th enrichment. They also have similar (^{238}U/^{232}Th) regardless of their crystal content, age or composition. Significantly, the extent of disequilibrium, and therefore also (^{230}Th/^{232}Th), correlates with age. That is, the

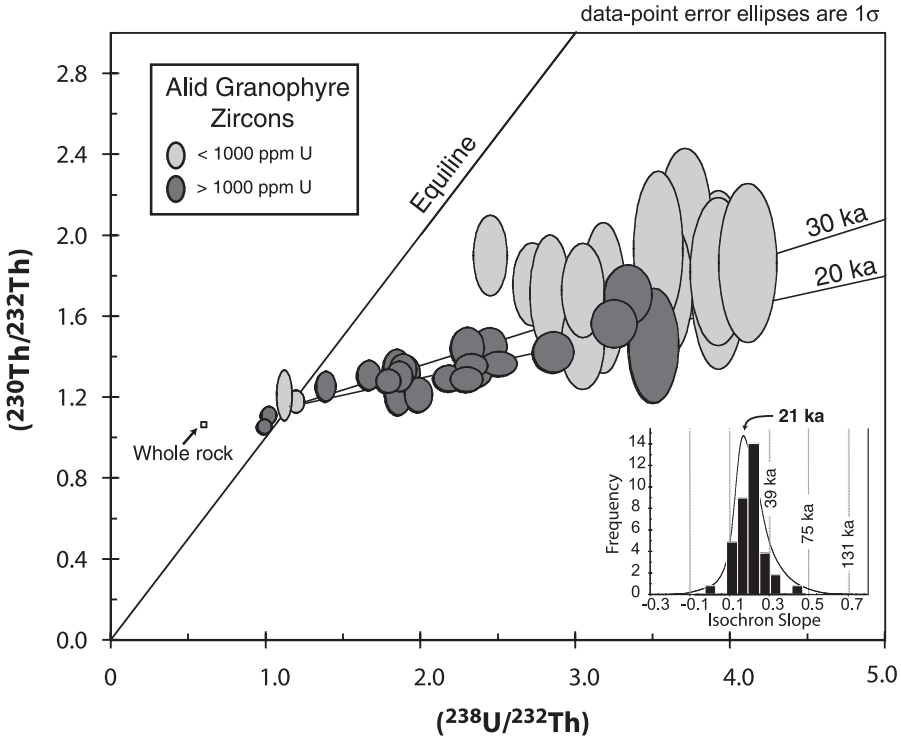

Fig. 5. Variation of ($^{238}U/^{232}Th$) vs ($^{230}Th/^{232}Th$) for multiple zircon analyses (by SIMS) from the granitic xenolith. Most zircons are consistent with crystallization at <50 ka. High-U spots give more precise ages that are seemingly younger. The histogram at the lower right shows the slopes of two-point isochrons between the zircon and the granophyre whole-rock composition. The peak of the associated maximum probability density curve, calculated by Isoplot (Ludwig, 2003*a*) yields an age of 21 ka.

Table 3: *U and Th concentrations and activities of mineral separates from Alid granophyre (*pf-inc, *C25)*

Type of material	WR	Apa	Mag	Feld	Pyx	Zirc(A)	Zirc(D)	Zirc(F)
U (ppm)	2·478	34·76	12·757	0·886	4·85	1104·9	1142·3	1087·3
±2σ	±0·003	±0·090	±0·047	±0·004	±0·020	±5·2	±12·9	±19·4
Th (ppm)	12·495	131·58	66·04	4·632	31·74	1765·7	1653·6	1677·8
±2σ	±0·099	±1·48	±0·37	±0·012	±0·416	±23·2	±25·5	±9·5
$(^{234}U/^{238}U)_{act}$	1·007	1·003	1·003	0·999	1·005	1·008	0·996	1·003
±2σ	±0·004	±0·004	±0·005	±0·006	±0·006	±0·007	±0·017	±0·025
Th/U	5·042	3·786	5·176	5·227	6·538	1·598	1·448	1·543
±2σ	±0·041	±0·044	±0·035	±0·029	±0·090	±0·022	±0·028	±0·029
$(^{238}U/^{232}Th)_{act}$	0·602	0·802	0·586	0·580	0·464	1·899	2·096	1·966
±2σ	±0·005	±0·009	±0·004	±0·003	±0·006	±0·027	±0·04	±0·037
$(^{230}Th/^{232}Th)_{act}$	1·064	1·085	1·060	1·063	1·036	1·317	1·308	1·306
±2σ	±0·008	±0·007	±0·006	±0·006	±0·005	±0·011	±0·009	±0·009
$(^{230}Th/^{238}U)_{act}$	1·768	1·354	1·808	1·831	2·232	0·694	0·624	0·664
±2σ	±0·014	±0·009	±0·012	±0·013	±0·015	±0·006	±0·008	±0·013

U and Th concentrations by isotope dilution, and activity ratios by TIMS; both at the Open University. WR, whole-rock; Apa, apatite; Mag, magnetite; Feld, anorthoclase; Pyx, ferroaugite (pyroxene); Zirc, zircon in three different separates.

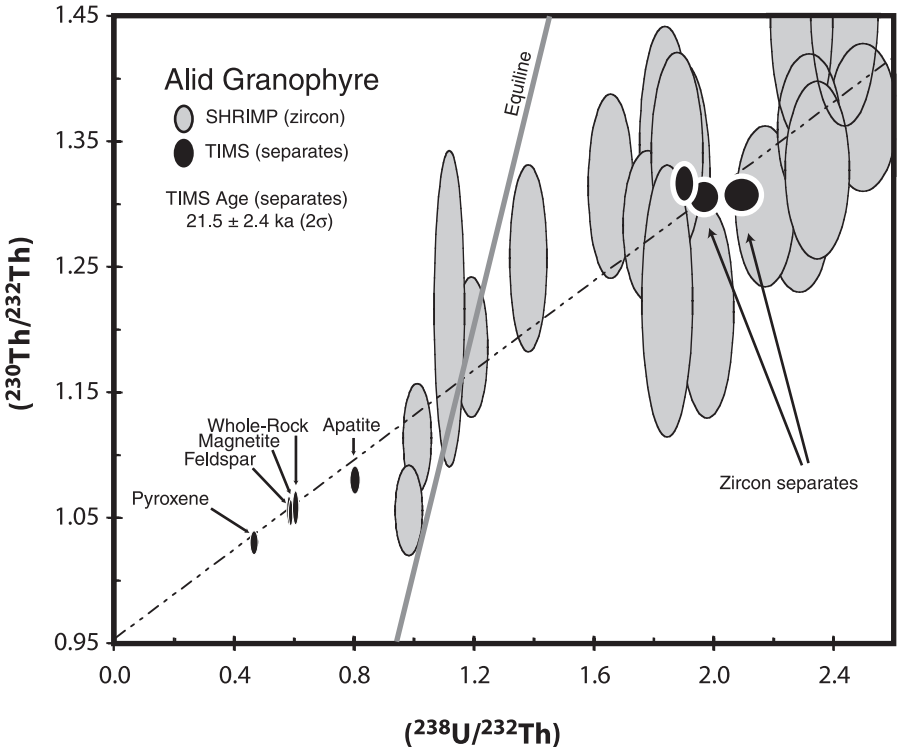

Fig. 6. Variation of (^{238}U/^{232}Th) vs (^{230}Th/^{232}Th) for SIMS analyses of individual zircons (gray ellipses) and TIMS bulk analyses of mineral separates from the granitic xenolith. The TIMS data form an isochron of 21·5 ± 2·4 ka, consistent with the zircon ages, implying that all crystallization occurred shortly prior to eruption and ejection of the xenolith.

young basalts have high (^{230}Th/^{232}Th), whereas the older basalts and rhyolites have lower (^{230}Th/^{232}Th). This implies that the basalts and rhyolites may be closely related (Hawkesworth *et al.*, 2001).

The simplest explanation would be that the rhyolites are related to the basalts by simple crystallization and differentiation, consistent with linear trends for incompatible trace elements (Fig. 8) and the small shifts in radiogenic isotope composition from basalt to rhyolite (Fig. 9). The basalts themselves have ^{230}Th enrichment, which is consistent with melting of an asthenospheric mantle source region and a garnet-bearing residuum that fractionates Th with respect to U (Asmerom, 1999; Bourdon & Sims, 2003). Migration of such basalts into the crust, and subsequent crystallization within the crust, would have allowed the rhyolitic melts to inherit the U/Th of the parental basalts. As time progressed, (^{230}Th/^{232}Th) decreased and trended toward the equiline as a result of radioactive decay, thereby creating the vertical trend observed in Fig. 7. U/Th ratios remained essentially unchanged by the decay of ^{230}Th alone. A change in the ratio only would have occurred if the fractionating assemblage strongly preferred one of these elements over the other.

As noted above, fractionation of U-rich zircon (and apatite) crystals during crystallization of the zircon-rich granophyre probably does account for the additional U/Th fractionation evident relative to its co-erupted pumice (Figs 7 and 8). However, the similar U/Th of all the rhyolitic units, regardless of their crystal content, argues against separation of zircon as the primary cause of ^{230}Th disequilibrium, as does the apparent lack of zircon in the volcanic rocks. The disequilibrium seems to be inherited at an earlier stage.

Time necessary for magma production

From these results, we conclude that the rhyolitic magmas from Alid had 'aged' for some time, causing (^{230}Th/^{232}Th) to decline with time at relatively constant U/Th (Thomas *et al.*, 1999; Hawkesworth *et al.*, 2001). In Fig. 10, we illustrate the time necessary to create the erupted rhyolites in the simplest scenario, starting with the composition of the local basalt. Basalts in the Afar region typically have (^{230}Th/^{232}Th) values of 1·15–1·30, as shown in Table 1 and by Vigier *et al.* (1999). If a basaltic magma with composition similar to those in Table 1 were to crystallize until 10–20% melt remained [i.e. F = 0·10–0·20, in the notation of DePaolo (1981)], it would produce a rhyolitic liquid with appropriate incompatible trace element compositions for the Alid rhyolites. For example, most

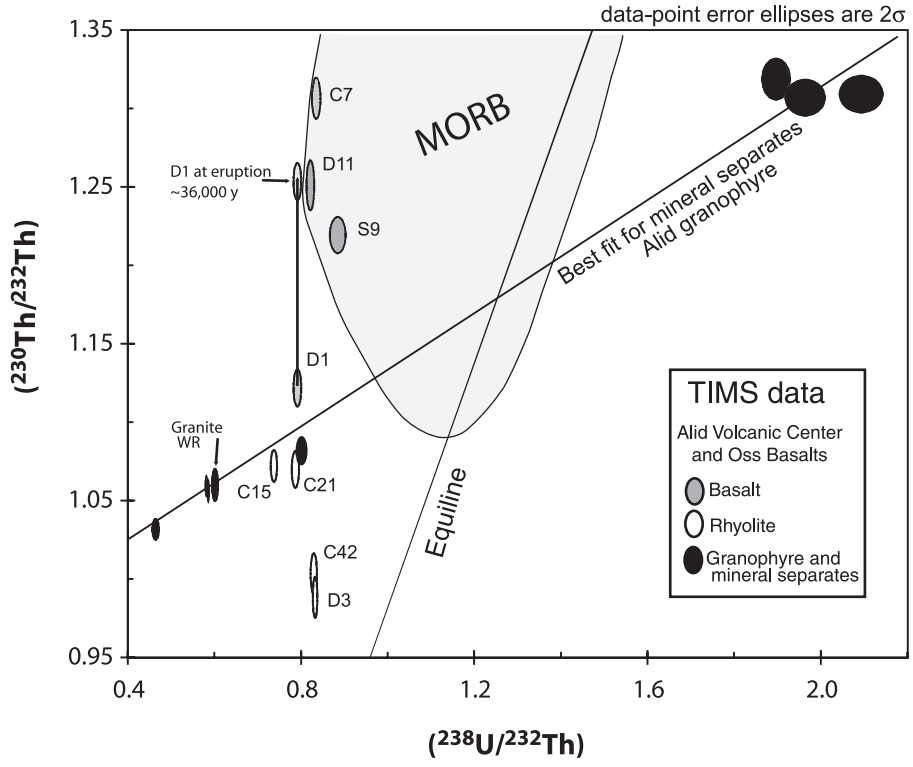

Fig. 7. Variation of ($^{238}U/^{232}Th$) vs ($^{230}Th/^{232}Th$) for TIMS analyses of whole-rock samples from the Alid volcanic center and the surrounding Oss basalt fields. The two rhyolitic whole-rocks associated with the 15·2 ka eruption (*pf*, C21 and C15) plot close to the isochron defined by mineral separates from the granitic xenolith. Two older rhyolites plot at lower ($^{230}Th/^{232}Th$). In contrast, most basalts plot at higher ($^{230}Th/^{232}Th$) but below values of 1·31. All basalts except D1 are expected to be Holocene in age. Present-day D1 is shown as its modeled ($^{230}Th/^{232}Th$) composition upon eruption at 36 ka. The whole-rock data are consistent with initial U–Th fractionation to produce the basaltic magmas, followed by aging and fractionation that do not affect the U–Th systematics of the volcanic rocks. Field for MORB is approximated from Lundstrom (2003, fig. 1).

nominally incompatible trace elements (Rb, U, Th, Pb, La) are enriched >5 times in the rhyolites relative to the more primitive basalts erupted in the region (Table 1, Figs 3 and 8). None is enriched more than tenfold. Simple mass balance calculations show that major element compositions of the rhyolites could be readily produced by 80–90% fractionation of observed mineral phases in the studied samples. Although the rock chemistries do not require a crystal-fractionation origin for the rhyolites, they are consistent with such an origin.

The time required to decay from a typical ($^{230}Th/^{232}Th$) of 1·30 for a basalt to the value for C21 (rhyolitic pumice) at the time of eruption (∼1·07) would be ∼50 000 years (track C in Fig. 10). From the same starting composition, sample C42, erupted some 20 000 years earlier, might have taken as long as 80 000 years to reach its ($^{230}Th/^{232}Th$) at the time of eruption. This scenario implies that 50 000–80 000 years are required for: (1) ascent of basaltic magma into the crust; (2) fractionation of crystals potentially accompanied by minor assimilation of crust; (3) intrusion into the shallow crust to form the Alid volcanic center and structural dome (including crystallization of the granophyre); (4) final eruption. The 50 000–80 000 years are maximum estimates, as the ($^{230}Th/^{232}Th$) values of some young basaltic rocks from the Afar are less than the values modeled above. Moreover, partial melting of continental crust and mixing with fractionating basalt would hasten the apparent decay toward the equiline and cause overestimation of the time since magma generation.

The effect of addition of old crust can be evaluated simply. The amount of assimilation can be constrained by the isotopic composition of the basalts, rhyolites and potential contaminants. The relatively similar Sr and Pb isotopic ratios of the basalts and rhyolites imply no more than about 5% assimilation of crust relative to fractionation of mafic precursors (Fig. 9). Near Alid and elsewhere in the world, old continental crust typically has low U/Th ratios and lies along the equiline at values between 0·6 and 0·9 (the bulk continental crust is 0·8; Rudnick & Fountain, 1995). Fractional melting of old crust could affect U/Th, but would not change ($^{230}Th/^{232}Th$), so that addition of such melts to a fractionating basalt could only drive the mixture down and potentially slightly to the left or right on Fig. 7.

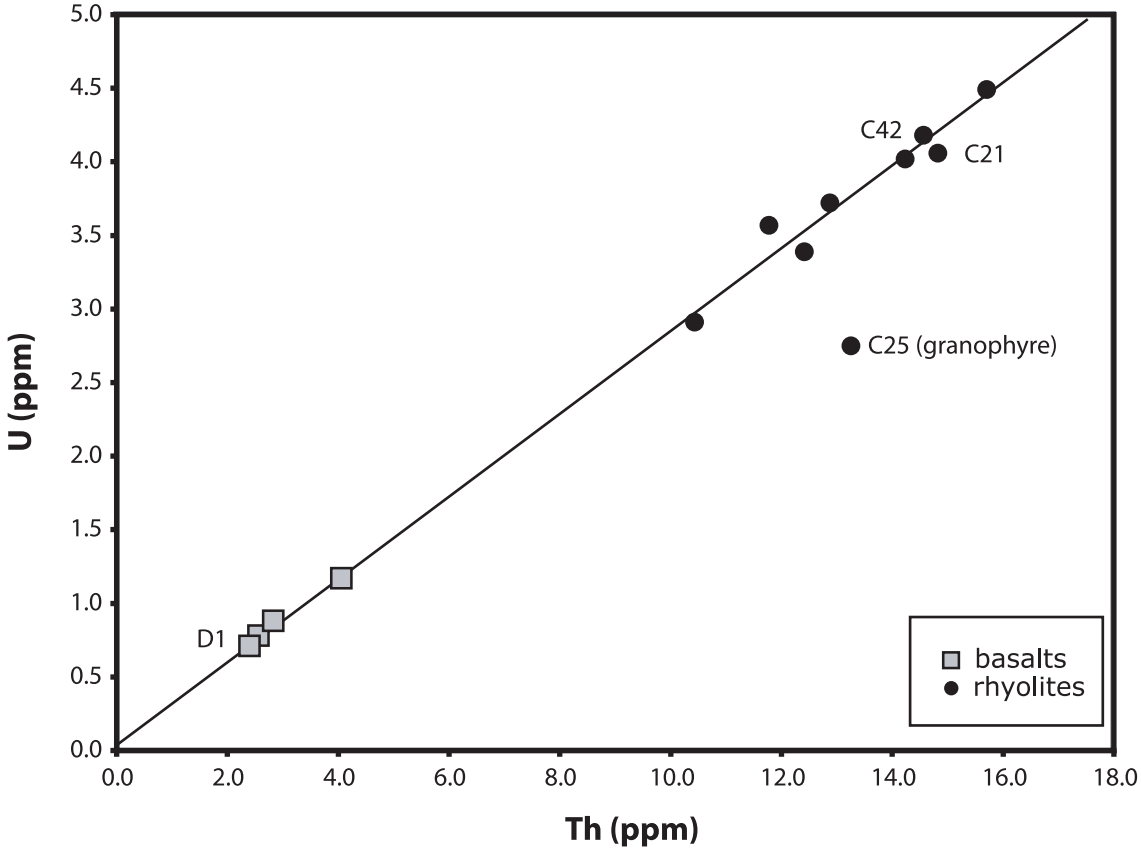

Fig. 8. U vs Th for rocks from the Alid volcanic center, as analyzed by ICP-MS [data from Duffield *et al.* (1997)]. Samples in Table 1 are labeled. C25 (the granophyre xenolith) plots away from the trend, showing some U loss, presumably as a result of zircon fractionation. All other rocks are collinear, consistent with comagmatism. The error associated with each datum point is smaller than the associated symbol.

For example, Trend B in Fig. 10 models the effects of assimilation–fractional crystallization (AFC) combined with radioactive decay. It shows evolution of a basalt with (^{230}Th/^{232}Th) of 1·3, which incrementally assimilates equilibrium crustal melt with (^{230}Th/^{232}Th) of 0·8 and Th concentration of 5 ppm. Using the AFC equations of DePaolo (1981) combined with the radioactive decay, the magma reaches the (^{230}Th/^{232}Th) of the C21 rhyolite in 43 000 years, about 6000 years faster than without crustal assimilation. If the assimilation was accomplished during the initial intrusion of basalt into the crust (the first 5000 years), then it would cause an initial decrease of (^{230}Th/^{232}Th) to 1·2, and the eruption value would be reached in about 30 000 years. Presumably, a scenario somewhere between A (progressive assimilation) and B (early assimilation) would be most likely.

Assimilation of Quaternary mafic crust could cause a similar drop in (^{230}Th/^{232}Th) and would cause far less shift in the Sr or Pb isotopes of the rhyolite. Consequently, the mass fraction of required assimilant (at equilibrium) would be greater, hastening the drop in the Th isotope ratio and allowing less time for fractionation than that calculated above for old continental crust.

Petrogenetic alternatives to fractionation of basalt

Another plausible origin for the rhyolites would be by melting of young (e.g. late Tertiary or early Quaternary) gabbros in the lower crust. If crustal melting were the primary means of magma generation, the Sr, Nd and Pb isotopic ratios require that the source be young and similar in composition to present-day basalts of the region (Fig. 9). However, previously intruded gabbros, unless they were extremely young (less than 300 000 years) would necessarily have (^{230}Th/^{232}Th) lower than their original mantle source region. If they represented mafic melts with similar U/Th to those sampled in this study, they would now reside on the equiline at (^{230}Th/^{232}Th) of ~0·8, which is less than the value for the rhyolites. Melting of such gabbros could, therefore, not create rhyolitic magma with a (^{230}Th/^{232}Th) of 1·1. Presumably, higher-degree melting of the mantle than created the Oss basalts would produce basalts with higher U/Th (small crystal/melt partition coefficients for U and Th require very low degrees of partial melting to create considerable disequilibrium; Lundstrom, 2003). During crystallization to form gabbros, the

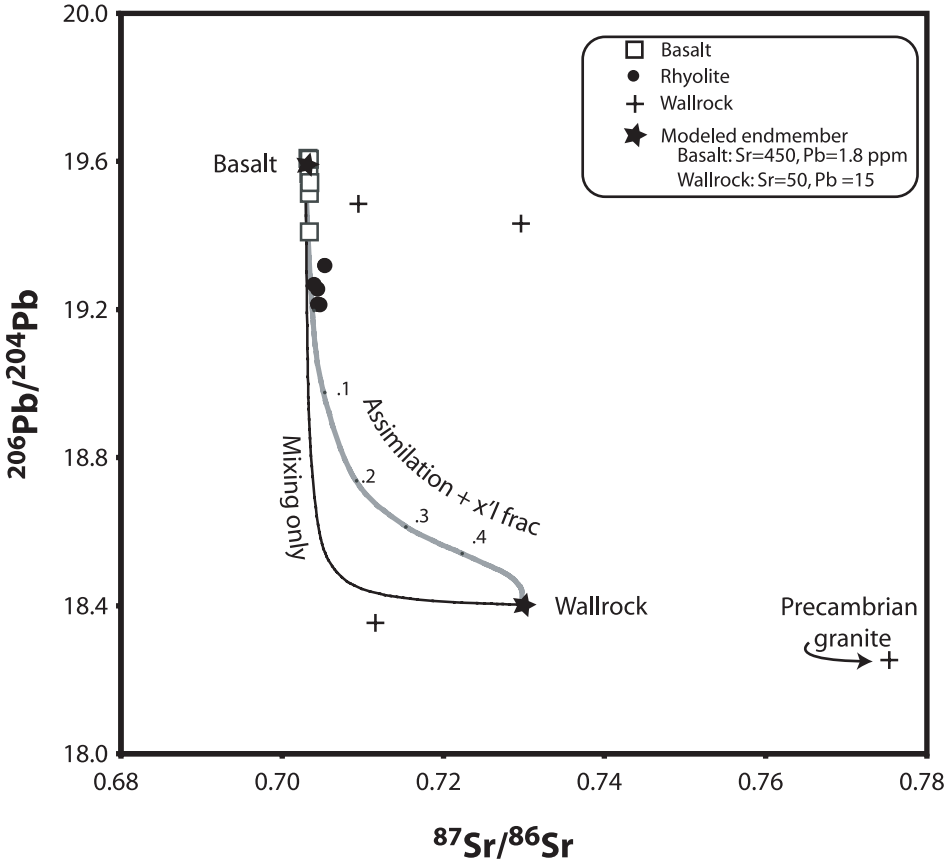

Fig. 9. Variation of $^{206}Pb/^{204}Pb$ vs $^{87}Sr/^{86}Sr$ for basalts, rhyolites and basement rocks at and in the vicinity of the Alid volcanic center. The basement rocks are isotopically and chemically diverse and include Precambrian granitoids. A simple AFC model [combined assimilation + fractional crystallization; DePaolo (1981)] is consistent with less than 10% assimilation of a hypothetical basement rock (star at lower right) during crystal fractionation of basalt. The mixing line represents simple mixing between the two end-members. The AFC curve shows crystal fractionation ($F = 0{\cdot}85$ or 85%) combined with assimilation, where the numbers next to the curve represent values of r (the ratio of mass fraction of assimilant to fractionated crystals). Wallrocks are all muscovite–kyanite schists except for the labeled Precambrian granite [data from Duffield *et al.* (1997)]. The modeled crustal end-member is a mixture of the two basement rocks with low $^{206}Pb/^{204}Pb$. Values of bulk D (2 for Sr and 0·4 for Pb) were chosen to replicate the concentrations of these elements in the rhyolite. Initial Sr and Pb concentrations for the basaltic end-member are from Duffield *et al.* (1997).

($^{230}Th/^{232}Th$) of these higher-degree melts would decline to values of 1·2 or less. If so, when subsequently melted, the new magma would have to form (fortuitously) with the same U/Th ratio as that of the basalts and rhyolites near Alid. The entire process of melt extraction, migration and crystallization would have to occur in 10 000–25 000 years, less time than for crystal fractionation of mantle-derived basalt combined with assimilation of old crust (modeled above), and less time than for crystal fractionation of the basalt alone. Melting of very young gabbro (<100 000 years old) could fit the time constraints of the U–Th data, but at some point the conceptual and practical boundaries between remelting of young gabbro and crystallization of young basalt becomes blurred.

A completely different possibility might be recharge of recently produced rhyolitic magma that could back-mix with the Alid silicic magma reservoir and raise the ($^{230}Th/^{232}Th$) of the silicic magma chamber toward values more representative of the basaltic parent (e.g. Hughes & Hawkesworth, 1999). In such a scenario, the magma would be prevented from losing its U–Th disequilibrium and would appear to have fractionated more quickly than actually occurred. That is, our estimates for the time of fractionation would be less than the actual time involved. This situation seems unlikely for at least two reasons. First, there is little petrographic evidence for repeated mixing and temperature cycling in any of the rhyolites; crystals are euhedral and minimally zoned. Second, the system is small-volume (5–50 km^3) and not the sort of large integrated magmatic system that might allow repeated interception of new magma batches. The two older rhyolite samples (C42 and D3) have lower ($^{230}Th/^{232}Th$)

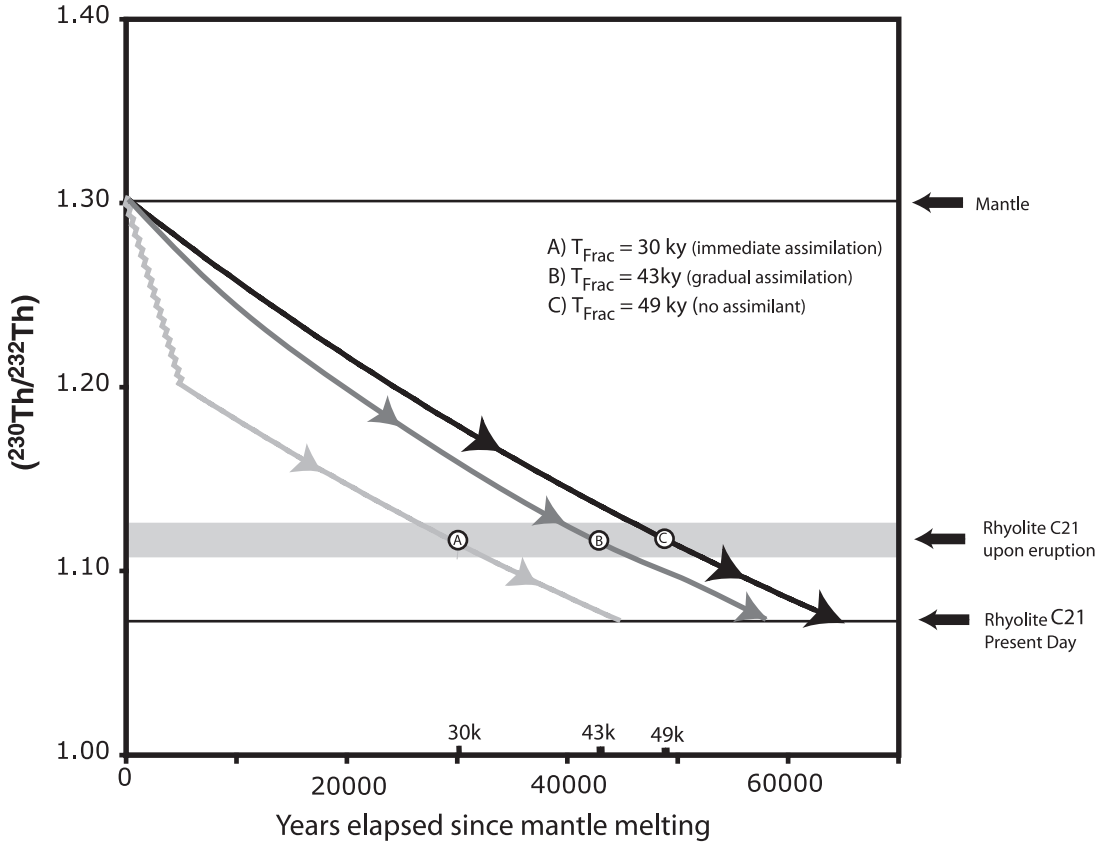

Fig. 10. Modeled change in (^{230}Th/^{232}Th) with time. U–Th fractionation during mantle melting creates mafic magmas with disequilibrium (^{230}Th/^{232}Th) close to values of 1·3 at (^{238}U/^{232}Th) of 0·8. Thorium isotopic ratios then decline during fractionation provided that U and Th are not subsequently fractionated (as can be inferred from the vertical array in Fig. 5). Basaltic melt would age to the value of the Alid rhyolite, *pf* (C21) at the time of its eruption in about 49 000 years (track C). Assimilation of continental crust would bring (^{230}Th/^{232}Th) down in less time (tracks A and B), potentially reaching the value of C21 at eruption in as little as 30 000 years (track A). Tracks A and B model assimilation of wall-rock on the equiline with (^{230}Th/^{232}Th) = 0·8 and a Th concentration of 5 ppm. Track A models full assimilation in the first 5000 years (zig-zag line) followed by fractionation and radiogenic decay (continuous line). Track B models gradual assimilation of wall-rock throughout the period of fractionation. Using the notation and equations from DePaolo (1981), we modeled a system with C_{lo} (for Th) = 2, $C^* = 5$, $F = 0{\cdot}15$, $r = 0{\cdot}05$ and $D = 0{\cdot}0001$. (See text for further details.)

than the granophyre and *pf* pumice and they also contain fayalite, consistent with independent magma batches rising separately and without homogenization. Early erupted *frhy1* and *frhy3* lavas are aphyric to sparsely phyric and distinct petrographically from the *pf* units.

Another mode of origin for rhyolites can be exfiltration (e.g. filter pressing) of crystal-poor melts from mush zones of intermediate-composition magmas in the mid-crust (e.g. Bachmann & Bergantz, 2004). Unlike in continental arcs, crystal-rich intermediate rocks are virtually absent in the Danakil Depression. Those andesites erupted at Alid, when present, are nearly aphyric. It therefore seems unlikely that large volumes of crystal-rich andesitic magmas are ponding beneath Alid. Moreover, it is difficult to envision how silicic melts with significant U–Th disequilibrium could be produced in such a geological environment. Most rhyolitic magmas formed in arc environments from intermediate-composition parents tend to have U–Th compositions at or near the equiline (Reagan *et al.*, 2003).

CONCLUSIONS

We consider that the simplest interpretation for the dataset is that crystal fractionation of young basalt produced the Alid rhyolites. The rhyolites could have formed by 80–90% crystallization of the kinds of basalts erupted regionally. The time estimates in this paper should be maxima, implying that the *pf* magma and entrained crystallized granophyre erupted less than 50 000 years after initial generation of their parent basaltic melts. Assimilation of ^{230}Th-equilibrated crust would cause overestimation of this time by 5000–20 000 years. Melting of gabbro in the crust would do the same, and would require fortuitous alignment of the U/Th ratios of basalts and rhyolites along

the range of (^{230}Th/^{232}Th). Accepting a genetic link between basalt and rhyolite, a fractionation rate can be estimated by dividing the magma fraction crystallized (~0·85) by the time period of differentiation, yielding rates between 2×10^{-5} and 3×10^{-5} per year. Such rates are comparable with those estimated for trachyte generation from hawaiite at Longonot volcano, Kenya (Rogers *et al.*, 2004), and production of peralkaline rhyolite at Olkaria, Kenya (Heumann & Davies, 2002), but slower than the shallow fractionation within basaltic suites shown by Vigier *et al.* (1999) and Cooper *et al.* (2001). Incorporating the estimated silicic magma volume (10–50 km^3), the production rate for rhyolitic magma was 2×10^{-4} to $1{\cdot}0 \times 10^{-3}$ km^3 per year.

ACKNOWLEDGEMENTS

Harold Persing helped collect the SIMS data on the USGS–Stanford SHRIMP RG. Tom Bullen and John Fitzpatrick analyzed samples for their isotopic compositions and trace element concentrations. Robert Oscarson assisted with the cathodoluminescence imaging of zircons. Isotope research at the Open University is partly supported by NERC, and we thank Peter van Calsteren and Jo Rhodes for their assistance. Tom Sisson and Charlie Bacon carefully reviewed an early draft of the manuscript. We appreciate excellent journal reviews by Arnd Heumann, Mark Reagan, Jorge Vazquez and Wendy Bohrson. The original fieldwork in Eritrea supported a geothermal assessment funded by the US Agency for International Development and the US Geological Survey.

REFERENCES

Allègre, C. J. (1968). ^{230}Th dating of volcanic rocks: a comment. *Earth and Planetary Science Letters* **5**, 209–210.

Asmerom, Y. (1999). Th–U fractionation and mantle structure. *Earth and Planetary Science Letters* **166**, 163–175.

Bachmann, O. & Bergantz, G. W. (2004). On the origin of crystal-poor rhyolites: extracted from batholithic crystal mushes. *Journal of Petrology* **45**, 1565–1582.

Bacon, C. R. & Lowenstern, J. B. (2005). Late Pleistocene granodiorite source for recycled zircon and phenocrysts in rhyodacite lava at Crater Lake, Oregon. *Earth and Planetary Science Letters* **233**, 277–293.

Bacon, C. R., Persing, H. M., Wooden, J. L. & Ireland, T. R. (2000). Late Pleistocene granodiorite beneath Crater Lake caldera, Oregon, dated by ion microprobe. *Geology* **28**, 467–470.

Berlo, K., Turner, S., Blundy, J. & Hawkesworth, C. (2003). The extent of U-series disequilibria produced during partial melting of the lower crust with implications for the formation of the Mount St. Helens dacites. *Contributions to Mineralogy and Petrology* **148**, 122–130.

Bindeman, I. N., Valley, J. W., Wooden, J. L. & Persing, H. M. (2001). Post-caldera volcanism: *in situ* measurement of U–Pb age and oxygen isotope ratio in Pleistocene zircons from Yellowstone caldera. *Earth and Planetary Science Letters* **180**, 197–206.

Black, S., Macdonald, R. & Kelly, M. R. (1997). Crustal origin for peralkaline rhyolites from Kenya: evidence from U-series disequilibria and Th isotopes. *Journal of Petrology* **38**, 277–297.

Blundy, J. & Wood, B. (2003). Mineral–melt partitioning of uranium, thorium and their daughters. In: Bourdon, B., Henderson, G. M., Lundstrom, C. C. & Turner, S. P. (eds) Uranium-Series Geochemistry. *Mineralogical Society of America Reviews in Mineralogy and Geochemistry* **52**, 59–123.

Bourdon, B. & Sims, K. W. W. (2003). U-series constraints on intraplate basaltic magmatism. In: Bourdon, B., Henderson, G. M., Lundstrom, C. C. & Turner, S. P. (eds) Uranium-Series Geochemistry. *Mineralogical Society of America Reviews in Mineralogy and Geochemistry* **52**, 215–248.

Bullen, T. D. & Clynne, M. A. (1990). Trace-element and isotopic constraints on magma evolution at Lassen volcanic center. *Journal of Geophysical Research* **95**, 19671–19691.

Charlier, B. L. A. & Zellmer, G. F. (2000). Some remarks on U–Th mineral ages from igneous rocks with prolonged crystallization histories. *Earth and Planetary Science Letters* **183**, 457–469.

Charlier, B. L. A., Peate, D. W., Wilson, C. J. N., Lowenstern, J. B., Storey, M. & Brown, S. J. A. (2003). Crystallization ages in coeval silicic magma bodies: ^{238}U–^{230}Th disequilibrium evidence from the Rotoiti and Earthquake Flat eruption deposits, Taupo Volcanic Zone, New Zealand. *Earth and Planetary Science Letters* **206**, 441–457.

Charlier, B. L. A., Wilson, C. J. N., Lowenstern, J. B., Blake, S., Van Calsteren, P. W. & Davidson, J. P. (2005). Magma generation at a large, hyperactive silicic volcano (Taupo, New Zealand) revealed by U–Th and U-Pb systematics in zircons. *Journal of Petrology* **46**, 3–32.

CNR–CNRS (1973), Geology of northern Afar (Ethiopia). *Revue de Geographie Physique et de Geologie Dynamique* **15**(4), 443–490.

Condomines, M., Hemond, Ch. & Allègre, C. J. (1988). U–Th–Ra radioactive disequilibria and magmatic processes. *Earth and Planetary Science Letters* **90**, 243–262.

Cooper, K. M., Reid, M. R., Murrell, M. T. & Clague, D. A. (2001). Crystal and magma residence at Kilauea Volcano, Hawaii: ^{230}Th–^{226} Ra dating of the 1955 east rift eruption. *Earth and Planetary Science Letters* **184**, 703–718.

DePaolo, D. J. (1981). Trace element and isotopic effects of combined wallrock assimilation and fractional crystallization. *Earth and Planetary Sciences* **53**, 189–202.

Duffield, W. A., Bullen, T. D., Clynne, M. A., Fournier, R. O., Janik, C. J., Lanphere, M. A., Lowenstern, J., Smith, J. G., Woldegiorgis, L., Kahsai, G., Weldemariam, K. & Tesfai, T. (1997). Geothermal potential of the Alid volcanic center, Danakil Depression, Eritrea. *US Geological Survey Open-File Report* **97–291**, 62 p.

Gill, J. B., Pyle, D. M. & Williams, R. W. (1992). Igneous rocks. In: Ivanovich, M. & Harmon, R. S. (eds) *Uranium-series Disequilibrium; Applications to Earth, Marine, and Environmental Sciences*. Oxford: Clarendon Press, pp. 207–258.

Harris, N., Vance, D. & Ayres, M. (2000). From sediment to granite: timescales of anatexis in the upper crust. *Chemical Geology* **162**, 155–167.

Hawkesworth, C. J., Turner, S. P. & Thomas, L. (2001). Magma differentiation rates: combining isotopic constraints and thermal models. *EOS Transactions, American Geophysical Union* **82**(24), 261–265.

Heumann, A. & Davies, G. R. (2002). U–Th disequilibrium and Rb–Sr age constraints on the magmatic evolution of peralkaline rhyolites from Kenya. *Journal of Petrology* **43**, 557–577.

Hughes, R. D. & Hawkesworth, C. J. (1999). The effects of magma replenishment processes on ^{238}U–^{230}Th disequilibrium. *Geochimica et Cosmochimica Acta* **63**, 4101–4110.

Layer, P. W. & Gardner, J. E. (2001). Excess argon in Mount St. Helens plagioclase as a recorder of magmatic processes. *Geophysical Research Letters* **28**, 4279–4282.

Lowenstern, J. B., Clynne, M. A. & Bullen, T. D. (1997). Comagmatic A-type granophyre and rhyolite from the Alid volcanic center, Eritrea, northeast Africa. *Journal of Petrology* **38**, 1707–1721.

Lowenstern, J. B., Janik, C. J., Fournier, R. O., Tesfai, T., Duffield, W. A., Clynne, M. A., Smith, J. G., Woldegiorgis, W., Weldemariam, K. & Kahsai, G. (1999). A geochemical reconnaissance of the Alid volcanic center and geothermal system, Danakil depression, Eritrea. *Geothermics* **28**, 161–187.

Lowenstern, J. B., Persing, H. M., Wooden, J. L., Lanphere, M. A., Donnelly-Nolan, J. M. & Grove, T. L. (2000). U–Th dating of single zircons from young granitoid xenoliths: new tools for understanding volcanic processes. *Earth and Planetary Science Letters* **183**, 291–302.

Ludwig, K. A. (2003a). *Isoplot/Ex ver. 3.00, A Geochronological Tool Kit for Microsoft Excel, Berkeley Geochronology Center Special Publications* **4**.

Ludwig, K. A. (2003b). Mathematical–statistical treatment of data and errors for ^{230}Th/U geochrology. In: Bourdon, B., Henderson, G. M., Lundstrom, C. C. & Turner, S. P. (eds) Uranium-Series Geochemistry. *Mineralogical Society of America Reviews in Mineralogy and Geochemistry* **52**, 631–666.

Lundstrom, C. C. (2003). Uranium-series disequilibria in mid-ocean ridge basalts: observations and models of basalt gensis. In: Bourdon, B., Henderson, G. M., Lundstrom, C. C. & Turner, S. P. (eds) Uranium-Series Geochemistry. *Mineralogical Society of America Reviews in Mineralogy and Geochemistry* **52**, 175–214.

Marini, A. (1938). Il Vulcano Alid nella Colonia Eritrea. *L'Universo* **19**, 51–65; **19**, 131–170.

McKenzie, D. (2000). Constraints on melt generation from U-series activity ratios. *Chemical Geology* **162**, 81–94.

Miller, J. S. & Wooden, J. L. (2004). Residence, resorption and recycling of zircons in Devils Kitchen rhyolite, Coso volcanic field, California. *Journal of Petrology* **45**, 2155–2170.

Paces, J. B. & Miller, J. D. (1993). Precise U-Pb ages of Duluth Complex and related mafic intrusions, northeastern Minnesota: Geochronological insights to physical, petrogenetic, paleomagnetic, and tectonomagmatic process associated with the 1.1 Ga Mid-continent Rift System. *Journal of Geophysical Research* **98**, 13997–14013.

Pearce, J. A. (1983). The role of sub-continental lithosphere in magma genesis at destructive plate margins. In: Hawkesworth, C. J. & Norry, M. J. (eds) *Continental Basalts and Mantle Xenoliths*. Nantwich: Shiva, pp. 230–249.

Petford, N., Cruden, A. R., McCaffrey, K. J. W. & Vigneresse, J.-L. (2000). Granite magma formation, transport and emplacement in the Earth's crust. *Nature* **408**, 669–673.

Reagan, M. K., Sims, K. W. W., Erich, J., Thomas, R. B., Cheng, H., Edwards, R. L., Layne, G. & Ball, L. (2003). Time-scales of differentiation from mafic parents to rhyolite in North American continental arcs. *Journal of Petrology* **44**, 1703–1726.

Reid, M. R. (2003). Timescales of magma transfer and storage in the crust. In: Holland, H. D. & Turekian, K. K. (eds) *Treatise on Geochemistry, 3*. Amsterdam: Elsevier, pp. 167–193.

Reid, M. R., Coath, C. D., Harrison, T. M. & McKeegan, K. D. (1997). Prolonged residence times for the youngest rhyolites associated with Long Valley caldera: ^{230}Th–^{238}U ion microprobe dating of young zircons. *Earth and Planetary Science Letters* **150**, 27–39.

Rogers, N. W., Evans, P. J., Blake, S., Scott, S. C. & Hawkesworth, C. J. (2004). Rates and timescales of fractional crystallization from ^{238}U–^{230}Th–^{226}Ra disequilibria in trachyte lavas from Longonot Volcano, Kenya. *Journal of Petrology* **45**, 1747–1776.

Rudnick, R. L. & Fountain, D. M. (1995). Nature and composition of the continental crust: a lower crustal perspective. *Reviews in Geophysics* **33**, 267–309.

Schmitt, A., Grove, M., Harrison, T. M., Lovera, O., Hulen, J. & Walters, M. (2003). The Geysers–Cobb Mountain magma system, California (Part 1): U–Pb zircon ages of volcanic rocks, conditions of zircon crystallization and magma residence times. *Geochimica et Cosmochimica Acta* **67**, 3423–3442.

Thomas, L., Hawkesworth, C., Van Calsteren, P., Turner, S. & Rogers, N. (1999). Melt generation beneath ocean islands: a U–Th–Ra isotope study from Lanzarote in the Canary Islands. *Geochimica et Cosmochimica Acta* **63**, 4081–4099.

van Calsteren, P. W. & Schweiters, J. B. (1995). Performance of a thermal ionisation mass spectrometer with a deceleration lens system and post-deceleration detector system. *International Journal of Mass Spectrometry and Ion Processes* **146–147**, 119–129.

Vazquez, J. A. & Reid, M. R. (2002). Time scales of magma storage and differentiation of voluminous high-silica rhyolites at Yellowstone caldera, Wyoming. *Contributions to Mineralogy and Petrology* **144**, 274–285.

Vigier, N., Bourdon, B., Joron, J. L. & Allègre, C. J. (1999). U-decay series and trace element systematics in the 1978 eruption of Ardoukoba, Asal rift: timescale of magma crystallization. *Earth and Planetary Science Letters* **174**, 81–97.

Watson, E. B. & Harrison, T. M. (1983). Zircon saturation revisited: temperature and composition effects in a variety of crustal magma types. *Earth and Planetary Science Letters* **64**, 295–304.